JCTC Journal of Chemical Theory and Computation

Molecular Dynamics Simulations of the Orientation of Ni(II)•Gly-Gly-His and Ni(II)•Arg-Gly-His Metallopeptide−DNA Association

Ya-Yin Fang,[§] Kenny B. Lipkowitz,[‡] and Eric C. Long*,[†]

Department of Biochemistry and Molecular Biology and Department of Chemistry, Howard University, 520 W Street, NW, Washington, D.C. 20059, and Department of Chemistry and Chemical Biology, Purdue School of Science, Indiana University—Purdue University Indianapolis (IUPUI), 402 North Blackford Street, Indianapolis, Indiana 46202-3274

Received February 21, 2006

Abstract: Ni(II)•Xaa-Gly-His metallopeptides (where Xaa is any α-amino acid) bind selectively to the minor groove of A/T-rich DNA regions as a function of their amino acid composition and chirality. Molecular dynamics simulations were performed to clarify the most likely binding orientations of Ni(II)•Gly-Gly-His and Ni(II)•L-Arg-Gly-His upon association with the B-form oligonucleotide d(CGCGAATTCGCG)$_2$. Upon examination of four possible docking orientations (**I**−**IV**), these studies indicated that both metallopeptides favor association with DNA via **I**, involving insertion of the edge of the metallopeptide containing the amino-terminal N−H and the imidazole pyrrole N−H group of His into the minor groove. These metallopeptide moieties play important roles in this DNA recognition mode by functioning as H-bond donors to minor groove acceptors such as the N3 of adenine or the O2 of thymine located on the floor of the minor groove. The positively charged side chain of L-Arg was found to enhance DNA recognition relative to that exhibited by Ni(II)•Gly-Gly-His through an increased electrostatic interaction, its favorable stereochemistry, and by providing a third point of contact with the minor groove floor. The simulation of orientation **I** was found to reproduce the experimentally supported DNA−metallopeptide orientation, revealing factors that are important for the further development of DNA-binding ligands.

Introduction

Sequence-selective DNA minor groove binding ligands are of ongoing interest due to their ability to act as nucleic acid conformational probes, footprint reagents, and antitumor or antiparasitic drugs.[1−4] In this general area, metallopeptides such as M(II)•Gly-Gly-His (where M = Cu or Ni) have attracted attention as DNA-interactive agents because they display the same chemical functional groups employed by proteins or peptide-derived natural products for DNA and RNA recognition.[5,6] In addition, the metal center of a metallopeptide produces a well-defined complex shape while also giving the peptide redox reactivity, enabling metallopeptides to cleave nucleic acids oxidatively in a fashion reminiscent of the bleomycin group[7] of clinically employed antitumor agents. Indeed, recent results indicate that these systems are very efficient single-[8] and double-strand[9] DNA cleavage agents (via C4′−H abstraction) and, earlier, that Cu(II)•Gly-Gly-His displays activity against Ehrlich ascites tumor cells.[10] Metallopeptides derived from the basic Gly-Gly-His peptide thus provide models for the study of fundamental DNA-small molecule interactions.[5,6,11]

* Corresponding author phone: (317)274-6888; fax: (317)274-4701; e-mail: long@chem.iupui.edu.

[†] IUPUI.

[‡] Department of Chemistry, Howard University.

[§] Department of Biochemistry and Molecular Biology, Howard University.

10.1021/ct600074r CCC: $33.50
Published on Web 07/29/2006

To date, studies of M(II)•Gly-Gly-His-derived metallopeptides have focused on their ability to recognize and cleave DNA.[5,6] Through a variety of experimental techniques it has been determined that these systems orient stereospecifically[12,13] in the DNA minor groove and that Ni(II)•Gly-Gly-His displays a slight preference for A/T-rich DNA regions;[14] however, DNA cleavage becomes more efficient and focused to A/T-rich regions when Arg and Lys, containing positively charged side chains, are included in the tripeptide ligand.[14] DNA cleavage recognition is also altered by the stereochemistry of the amino acids present in the tripeptide ligand. For example, recent experimental studies have shown that Ni(II)•L-Arg-Gly-His has an increased and altered DNA site-selectivity relative to Ni(II)•D-Arg-Gly-His.[15]

Unfortunately, information concerning the exact orientation of DNA−metallopeptide association, and factors leading to their efficient DNA cleavage, is still insufficient due to a lack of high-resolution structures and the dynamic nature of their DNA interaction. While experimental evidence available at the present time, including results from an NMR investigation,[13] point to a likely DNA binding orientation in which the His imidazole and terminal amine "edge" of each square-planar structure is inserted into the minor groove, alternative DNA association modes that are not detected by NMR cannot be definitively ruled out. Given the tetradentate fashion in which the central metal ion is bound through the amino terminal amine, two intervening, deprotonated peptide nitrogens, and the His imidazole,[16] each side of the square planar complex formed exposes several combinations of functional groups that could potentially mediate an alternative interaction with DNA. It is thus difficult to identify unambiguously which of four possible edges of the equatorial plane of a Ni(II)•Gly-Gly-His-derived complex inserts into the minor groove and which atoms interact with the floor of the minor groove. Further, without knowledge of a well-defined DNA binding orientation, it is difficult to assess the origin of the site-selectivities observed and how DNA cleavage activity is enhanced in some cases.

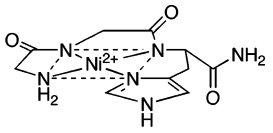

Ni(II)•Gly-Gly-His

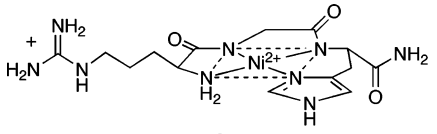

Ni(II)•Arg-Gly-His

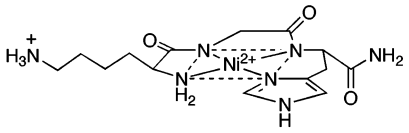

Ni(II)•Lys-Gly-His

To address these questions, four potential minor groove association modes of two metallopeptides were investigated and compared for the first time through molecular dynamics simulations using Ni(II)•Gly-Gly-His, the least substituted metallopeptide, and Ni(II)•L-Arg-Gly-His, which displays enhanced A/T site-selectivity. To probe and compare their most likely DNA binding orientations, these metallopeptides were docked without constraints into the minor groove of DNA in four possible orientations as defined in Scheme 1. These two particular metallopeptides were chosen for this examination because they have been studied experimentally;[5,6] therefore, information exists to guide and validate the interpretation of the simulations presented herein.

Scheme 1. Binding Orientations Employed upon Metallopeptide-Minor Groove Docking

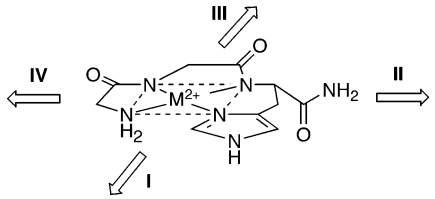

As will be presented, our simulations indicate that the most likely Ni(II)•Xaa-Gly-His metallopeptide-minor groove binding orientation is **I**, in which the N−H group of the His imidazole plays an important role in DNA recognition by functioning as an H-bond donor to the floor of the minor groove. In this orientation, the amino-terminal N−H protons assist in the recognition process in a fashion dependent upon the stereochemistry and identity of the amino acid present in this terminal residue. When present, a positively charged Arg residue assists in maintaining the favored binding orientation and enhances DNA association relative to Gly through an increased electrostatic interaction and by providing a third transient point of contact with the DNA. In the favored orientation (**I**) the simulations also support the DNA−metallopeptide orientation suggested through previous NMR studies.[13] In addition, new insights into the origins of the observed C4′−H abstraction chemistry, leading to direct DNA strand scission, were revealed. Overall, these studies have disclosed factors that are involved in metallopeptide−DNA association and impact the development of DNA binding ligands, in general. Perhaps as important, these studies provide an example to indicate that the judicious use of MD simulations can lead to meaningful insights pertaining to drug−DNA orientation phenomena in the absence of abundant experimental data.

Methods

General Considerations. Molecular modeling and molecular dynamics simulations of Ni(II)•Gly-Gly-His and Ni(II)•L-Arg-Gly-His bound to the minor groove of d(CGCGAATTCGCG)$_2$ were carried out using the protocols employed by Wellenzohn and co-workers.[17−19] Calculations were performed on an SGI Octane using MacroModel 7.4,[20] SPARTAN 5.11,[21] and AMBER 7.[22] Default settings for these programs were used unless specified otherwise. Force-field parameters for the tripeptide ligand bound to Ni^{2+} were developed as reported elsewhere;[13] these force-field parameters were derived from a crystallized Gly-Gly-His metallopeptide by optimizing missing parameters until the RMS deviation between the calculated and observed structure was

Table 1. Box Dimensions, Number of Waters, and Γ Values of Each Simulation

system	binding orientation	box dimension (Å)			number of waters	Γ value
		X	Y	Z		
DNA-Ni(II)•Gly-Gly-His	**I**	47.67	69.33	60.81	4810	200.41
	II	49.75	69.70	59.63	4951	206.29
	III	49.75	68.06	64.48	5232	218.00
	IV	51.73	67.01	62.33	5303	220.95
DNA-Ni(II)•L-Arg-Gly-His	**I**	57.63	69.84	50.12	4871	202.95
	II	54.78	67.01	65.03	5822	242.58
	III	51.04	68.06	63.40	5783	240.96
	IV	56.74	67.26	61.99	5847	243.62

minimized. As reported previously, the RMS deviation between the crystal structure and the AMBER minimized structure for those charges and geometry parameters is 0.257 Å, and the average RMS deviation between the X-ray structure and the computed structure along the testing simulation for those charges and geometry parameters is 0.283 Å. While there are no guarantees that the existing parameter set is optimal, as noted previously, the molecular dynamics simulations of the DNA−metallopeptide complex with the AMBER force field and the parameter set for Ni(II)•Gly-Gly-His not only generated adequate structural information without major structural deformations but also yielded reliable relative binding energies which corresponded to the site selectivities exhibited by the different metallopeptides and DNA.[13]

Starting Structures. Taking advantage of the noted similarities that occur between netropsin and Ni(II)•Xaa-Gly-His metallopeptides with regard to their A/T-rich site-selectivities and other features,[13] the crystal structure of netropsin-bound d(CGCGAATTCGCG)$_2$ (PDB reference code 1D86)[23] was used to create a minor groove binding site by replacing netropsin with Ni(II)•Gly-Gly-His or Ni(II)•L-Arg-Gly-His. The Ni(II)•Gly-Gly-His metallopeptide starting structure was derived from a crystal structure,[24] while that of Ni(II)•L-Arg-Gly-His was generated based on the same crystal structure of Ni(II)•Gly-Gly-His substituted appropriately in the first peptide position followed by molecular mechanics minimization; this substitution does not lead to changes in the rigid Ni(II)•Gly-Gly-His-like "core" of Ni(II)•Arg-Gly-His. The assembly of each DNA−metallopeptide complex was accomplished by docking a metallopeptide manually at the dyad axis of the oligonucleotide substrate in one of the four orientations defined in Scheme 1. Bump-checking was turned on to ensure that no overlapping atoms resulted during the docking process. Subsequently, each assembled metallopeptide−DNA complex was exported to AMBER. Given that each strand of DNA has 11 PO_4^- and Ni(II)•L-Arg-Gly-His possesses one positive charge, to achieve electroneutrality, 22 and 21 Na^+ counterions were added separately to the DNA-Ni(II)•Gly-Gly-His and DNA-Ni(II)•L-Arg-Gly-His complex systems, respectively, through use of the add-Ions command in the Xleap facility of AMBER. Solvation with TIP3P water boxes (resulting in a 10 Å solvent shell in all directions) completed each system. Table 1 lists the dimensions, number of waters, and corresponding relative Γ values (water/nucleotide) for each system studied.

Molecular Dynamics Simulations. The docked metallopeptide−DNA complexes described earlier, with associated Na^+ ions and water bath, were energy-minimized through 500 steps of a conjugate gradient, with 100 kcal (mol•Å)$^{-1}$ restraints on the DNA and counterion positions. During the following three, 500-step minimizations, the restraints were relaxed stepwise by 25 kcal (mol•Å)$^{-1}$ per step. Thus, the fifth, 500-step minimization was performed without restraints. Each optimized structure was heated from 100 to 300 K over a time period of 125 ps (with a temperature coupling of 0.2 ps), while positional restraints of 100 kcal(mol•Å)$^{-1}$ were used for the DNA and the counterions. A constant volume was maintained during this process. Subsequently, three sequential 25 ps MD steps at 300 K were carried out accompanied by the gradual loosening of restraints at a rate of 25 kcal(mol•Å)$^{-1}$ per step. The resulting restraint-free systems were allowed to equilibrate for an additional 15 ps; the temperature was allowed to fluctuate around 300 K with a temperature coupling time of 0.2 ps, and the pressure was allowed to fluctuate around 1 bar with a pressure coupling of 0.2 ps. Finally, production runs in excess of 1400 ps were carried out following this protocol. For each simulation, 5000 structures were saved to disk for postprocessing by uniformly sampling the trajectory during the production run. All analyses were carried out using the CARNAL and ANAL programs in AMBER.

MM Energies. Gas-phase molecular mechanical (MM) energies were averaged over all snapshots acquired between 500 and 1500 ps and included contributions from electrostatic and van der Waals interactions for the complex (DNA + metallopeptide), receptor (DNA), and ligand (metallopeptide). All MM calculations (AMBER) were performed with a nonbonded cutoff of 99 Å and a dielectric constant of 1 in the absence of any solvent or counterions. The receptor and ligand geometries were taken from those of the complex, and thus there is no internal energy contribution (i.e., from bonds, angles, and dihedrals) to the net MM average.

Potential Sources of Error. Potential errors in our computational methods that could influence the results of this study are worthy of note. The first possible error is the potential function itself. No force field is perfect, and they all have inherent errors. In this study, however, we have carried out simulations on exactly the same guest molecule (metallopeptide) binding to the same host (DNA) in the same binding site but with different docking orientations. Hence if the force field underestimates, for example, hydrogen bonding or overestimates electrostatic effects, it does so for

all orientations, thus leading to a cancellation of errors and providing meaningful relative energies. The next possible error to consider is that the simulation times, albeit quite lengthy in terms of CPU time (multiple weeks per trajectory), correspond to exceedingly short times in reality. In this study we probed energies, structures, and dynamical features on the nanosecond time scale, and that might be a source of error. However, we note that in structures we deem as being stable docking orientations the guest remains bound to the host for the entire trajectory, but, for unstable orientations, the guest dissociates from the DNA and migrates away from its docking site or it reorients itself from that unstable orientation to the stable orientation. Hence, we are observing important structural transitions within the simulation time period even though this time period is brief. Finally, we point out that by selecting another water potential or a different force field or a different set of simulation conditions, it is possible that we could derive different results from those presented here. However, previous simulation results using the same methods were found to be fully consistent with NOE data showing which protons of the metallopeptide are adjacent to a given set of protons on the DNA, and the results are consistent with other experimental results, the most notable of which is the agreement with the DNA degradation results described in an earlier paper.[15] Hence we summarize by noting that while possible errors could influence the results, those errors are marginal in scope and the computational protocols we have implemented have provided results that are consistent with experimental facts and allow us to extract meaningful information that is not amenable to experimentation.

Result and Discussion

Initially, the root-mean-square deviations (RMSDs) observed for each simulation were examined to determine if each system had attained equilibrium. The RMSDs of each DNA-Ni(II)•Gly-Gly-His and DNA-Ni(II)•L-Arg-Gly-His complex system, with respect to their starting structures, attained equilibrium after 250 ps, and their energies were found to be stable during the course of the remainder of each simulation. Hence, a time of 500 ps after thermal warm-up was selected as a starting point for data collection and for the analysis of each simulation.

Simulations of DNA + Ni(II)•Gly-Gly-His. Small RMSD values of each metallopeptide−DNA complex indicate stable structures. Figure 1 shows that the stabilities of the DNA-Ni(II)•Gly-Gly-His complexes initiated from orientations **I**, **II**, and **IV** were comparable during the simulations. In particular, with **I** and **IV**, the RMSDs of the DNA−metallopeptide complexes changed within the same range (2.0−4.0 Å). Worthy of note, the RMSDs observed for the complex initiated from **I** changed in a somewhat narrower range (2.5−3.5 Å), suggesting that the structure of this particular complex had less fluctuation during the course of the simulation.

Visual analysis of each trajectory obtained from these four simulations supports the general observations described above. When the simulation was initiated from orientation **I**, Ni(II)•Gly-Gly-His was found to maintain the key

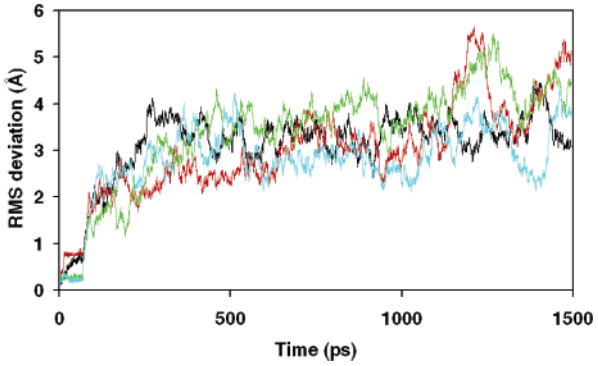

Figure 1. RMS deviations with respect to the starting structure in the simulation of Ni(II)•Gly-Gly-His bound to d(CGCGAATTCGCG)$_2$ in four orientations: **I**, black; **II**, red; **III**, green; and **IV**, blue.

characteristics of its starting structure. More specifically, (1) Ni(II)•Gly-Gly-His remained located at the dyad of the A/T-rich minor groove region; (2) the Ni(II) ion remained in close proximity to the C4′−H's of the nearest thymine residues on both antiparallel strands of the oligonucleotide; and (3) the equatorial plane of the metallopeptide remained parallel to the walls of the minor groove. However, while positioned as such, the metallopeptide−DNA complex initiated in **I** displayed dynamic motions relative to the DNA. Of note, Ni(II)•Gly-Gly-His was observed to rotate clockwise and counterclockwise around the C_n axis of the central Ni(II) ion of the complex. This clockwise and counterclockwise rotation produced changes in the identity and number of functional groups employed in the metallopeptide-minor groove interaction; that is, the starting structure alternated from an initial structure (**I**) in which the amino-terminal N−H and the pyrrole N−H of the His imidazole were involved simultaneously in minor groove binding [which takes place as single H-bonding events formed by the amino-terminal N−H (39% of the simulation time) as well as simultaneous multiple H-bonding events (simultaneous double and simultaneous triple H-bonds, 11% of the simulation time)] to structures involving either the amino-terminal N−H alone (21% of time) or the carboxy-terminal amide alone (22% of time). These two latter structures are similar to the starting structures assembled for orientations **IV** and **II**, respectively. Thus, Ni(II)•Gly-Gly-His remains in the center of the A/T-rich region and rocks back and forth between orientations that resemble the starting orientations defined previously as **II** and **IV**.

Similar to the above, when the simulation of Ni(II)•Gly-Gly-His was initiated from **II**, the metallopeptide immediately turned from its starting position in the minor groove to an orientation that was analogous to **I**. Upon attainment of equilibrium after this reorientation, Ni(II)•Gly-Gly-His behaved dynamically as described above for the simulation initiated from **I**. Similarly, the simulation that was initiated from **IV** rotated toward orientation **I** and, upon equilibration, remained in this orientation and again behaved dynamically as described for orientation **I**. Contrary to these findings is the case for **III** where the ligand moved out of the minor groove, suggesting either a very weak attraction or a repulsion between host and guest in that orientation. In

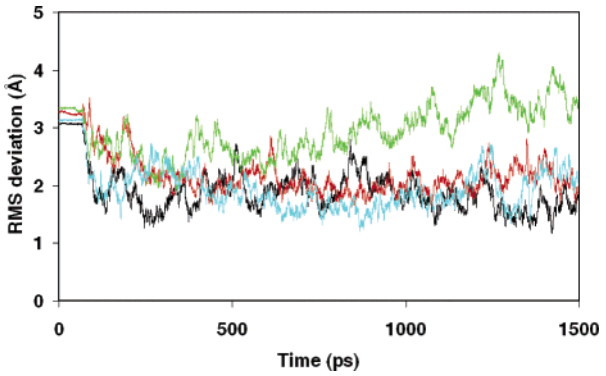

Figure 2. RMS deviations of Ni(II)•Gly-Gly-His bound to d(CGCGAATTCGCG)$_2$ in four directions (**I**, black; **II**, red; **III**, green; and **IV**, blue) with respect to the average structure generated in the simulation initiated from orientation **I**.

Table 2. Relative Binding Energies of DNA + Ni(II)•Gly-Gly-His[a]

orientation	$\Delta E_{complex}$[b]	ΔE_{DNA}[b]	ΔE_{ligand}[b]	$\Delta\Delta E$[c]
I	0	0	0	0
II	9	6.7	−3.9	6.2
III	88.5	−9.5	7.9	90.1
IV	−18.4	−26.3	7.7	0.2

[a] Energies are reported in kilocalories per mole. [b] $\Delta E_{complex}$, ΔE_{DNA}, and ΔE_{ligand} denote the molecular mechanical (MM) energies for the complex, DNA, and ligand, respectively, relative to orientation **I**. [c] Relative binding energies, calculated by $\Delta\Delta E = \Delta E_{complex} - \Delta E_{DNA} - \Delta E_{ligand}$.

support of these observations, Figure 2 illustrates the RMS deviations found for each of the above four DNA-Ni(II)•Gly-Gly-His simulations with respect to the average structure generated in the simulation resulting from **I**. This analysis shows that the simulations initiated from **I**, **II**, and **IV** all correspond quite closely to this particular final average structure, while aberrant behavior is noted from orientation **III**.

The above observations indicate that the most favored orientation of minor groove-bound Ni(II)•Gly-Gly-His initiates from an orientation as described for **I**. In this orientation, Ni(II)•Gly-Gly-His forms H-bonding interactions with the minor groove floor via the amino-terminal N−H protons and the pyrrole N−H of the His imidazole. However, with these initiating intermolecular contacts alone (in contrast to Ni(II)•L-Arg-Gly-His, as described later), the interaction between the DNA and the metallopeptide is not strong enough to hold this relatively small ligand in the minor groove firmly. As a consequence, the metallopeptide rotates as described. In addition, the relatively weak interactions that occur between Ni(II)•Gly-Gly-His and the minor groove also allow the metallopeptide to turn and take on this favored binding orientation even when it is docked initially via the adjacent edges of the equatorial plane (i.e., via **II** and **IV**).

The relative binding energies from each of the four simulations of Ni(II)•Gly-Gly-His (Table 2) are in good agreement with the qualitative observations made above. The simulation initiated from **I** has the lowest relative binding energy, and the simulation initiated from **III** has the highest relative binding energy; the relative binding energies of **IV** and **II** are close to the values found for **I**, with **IV** being slightly lower than **II**. In stark contrast, the energies determined as a consequence of binding orientation **III** were found to be much higher than those resulting from the other orientations. Indeed, over the lifetime of the trajectory measured, orientation **III** leads to a destabilizing, repulsive interaction.

Simulations of DNA-Ni(II)•L-Arg-Gly-His. Illustrated in Figure 3 are the four starting structures in orientations **I**−**IV** of DNA + Ni(II)•L-Arg-Gly-His as viewed from the side and above (orthogonal and parallel to the helix axis). In contrast to the starting structures assembled for Ni(II)•Gly-Gly-His, it is clear that the Arg side chain of Ni(II)•L-Arg-Gly-His introduces an extension that could either complement or complicate minor groove binding by the main equatorial plane of the metallopeptide; however, this appendage remains quite flexible and, as observed and noted below, only forms transient contacts with the DNA that are secondary to the main metallopeptide−DNA recognition elements: the His imidazole N−H and the terminal peptide amine N−H. The representations in Figure 3 also emphasize the similarities and differences between these different binding orientations.

As in the analysis of Ni(II)•Gly-Gly-His, Figure 4 combines plots of the RMS deviations observed for simulations of DNA-Ni(II)•L-Arg-Gly-His oriented as starting structures in orientations **I**−**IV**. These results indicate that the DNA-Ni(II)•L-Arg-Gly-His system oriented initially as **I** exhibits the lowest RMSD, suggesting that this particular DNA−metallopeptide complex orientation is most stable throughout the simulation. In contrast, the complex oriented initially as **II** has the highest RMS value with a maximum deviation at ∼1000 ps indicating a relatively large structural change at this point in the simulation; the RMSD resulting from the simulations of metallopeptide binding initiated from **III** and **IV** were found to be intermediate between those observed for **I** and **II**.

Visual analyses of the trajectories from the four simulations of Ni(II)•L-Arg-Gly-His support the general observations described above and reveal dynamic details of their DNA-Ni(II)•L-Arg-Gly-His interactions. In the simulation initiated from **I**, Ni(II)•L-Arg-Gly-His was found to be stable in its starting orientation. The metallopeptide remained bound in the minor groove, and its motion paralleled the motions of the DNA backbone. At the same time, (1) the width of the minor groove narrowed at the dyad of the A/T-rich region and widened at the junction between the A/T and G/C base pairs, and (2) the positively charged Arg side chain was localized within the minor groove and interacted transiently with H-bond acceptors located on the floor of the groove. These observations are reminiscent of the results of similar studies performed with Hoechst 33258 and netropsin.[18]

In the simulation initiated from **II**, the coordination plane alone was inserted into the minor groove with the positively charged Arg side chain projecting away from the helix axis. Without a firm anchoring interaction with the minor groove, the relative long, positively charged side chain of Arg remained in motion, flexed at the surface of the DNA, and, at times, bent toward the minor groove. These translational movements account for the high RMSD values overall, and the bending motion contributed to the large RMSD observed

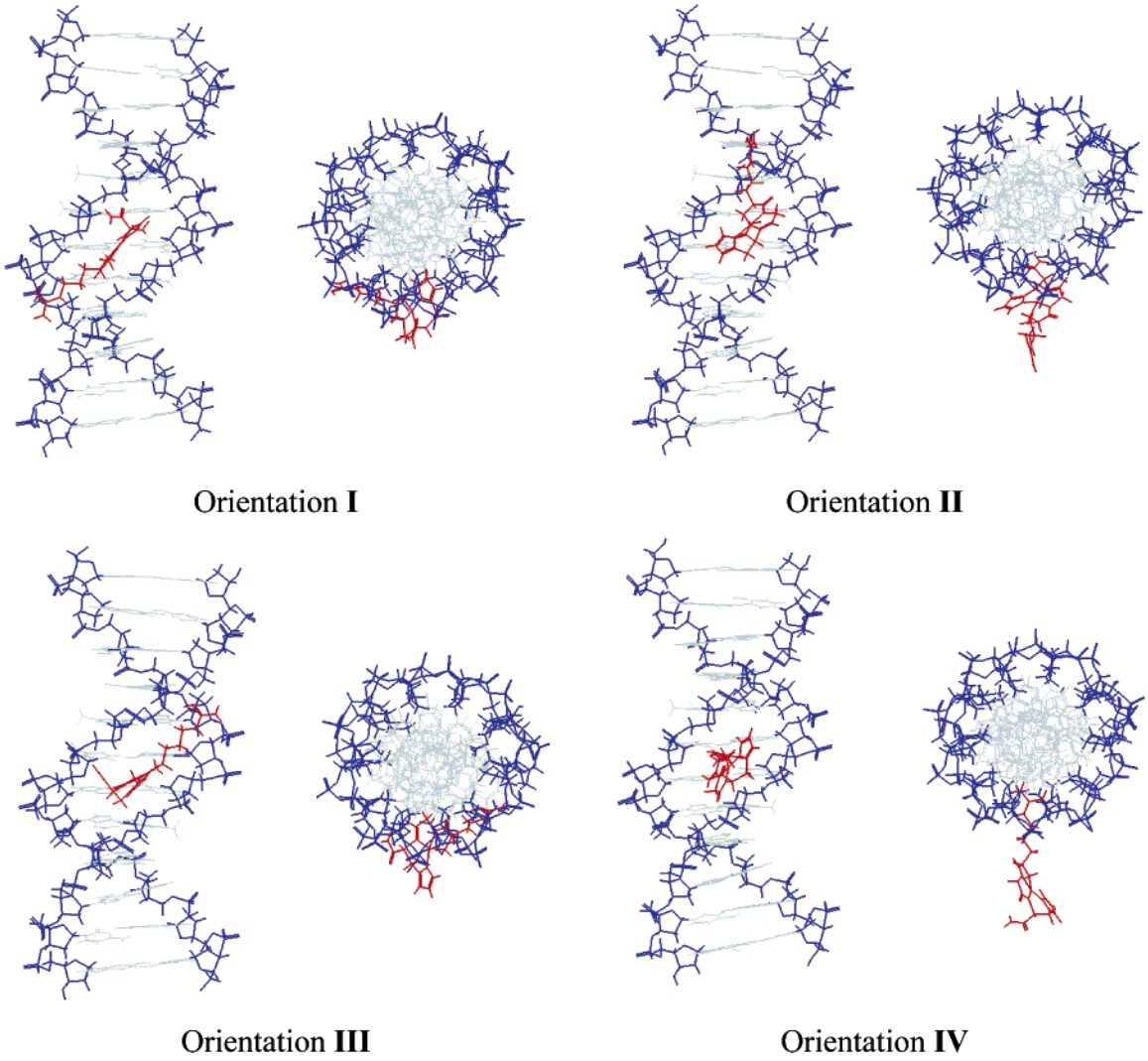

Figure 3. Starting structures of Ni(II)•L-Arg-Gly-His (red) bound to the minor groove of d(CGCGAATTCGCG)$_2$ in orientations **I**−**IV** as viewed orthogonal and parallel to the DNA axis.

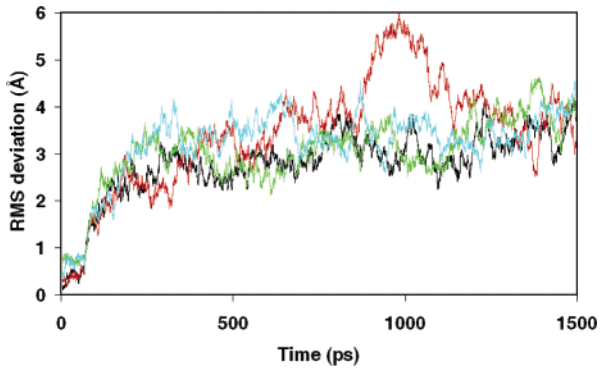

Figure 4. RMS deviations with respect to the starting structure in the simulations of Ni(II)•L-Arg-Gly-His bound to d(CGCGAATTCGCG)$_2$ in four starting orientations: **I**, black; **II**, red; **III**, green; and **IV**, blue.

at ∼1000 ps. In comparison to this is the simulation resulting from **IV** in which the positively charged side chain of Ni(II)•L-Arg-Gly-His was inserted into the minor groove, while the coordination plane was projecting outwardly from the minor groove. The results of this simulation were similar to those observed for **II**: The equatorial plane of the metallopeptide flexed at the end of the Arg side chain 'tether' and also bent, at times, toward the minor groove. However, because of the heavier mass associated with the metal complex core compared to the side chain, the movements of the projecting equatorial plane were slower and smaller and consequently did not result in a high RMSD as was found for **II**.

Finally, the simulation initiated from **III** revealed that this metallopeptide did not change its orientation within the simulation time with both the equatorial plane and the Arg side chain remaining in the minor groove; however, unlike the stable orientation observed as a result of orientation **I**, the metallopeptide bound initially as **III** interacted only at the surface of the minor groove and exhibited a strong tendency to move out of the groove. Also, in this simulation the DNA backbone was not affected as it was with **I** indicating a much lower extent of intermolecular interaction. The binding behavior of Ni(II)•L-Arg-Gly-His in orientation **III** is accounted for by the presence of the positively charged Arg side chain that helped to maintain the metallopeptide in proximity to the minor groove, a finding that is in contrast to the effect of orientation **III** found for Ni(II)•Gly-Gly-His, a charge-neutral system.

In a parallel analysis aimed at investigating and comparing

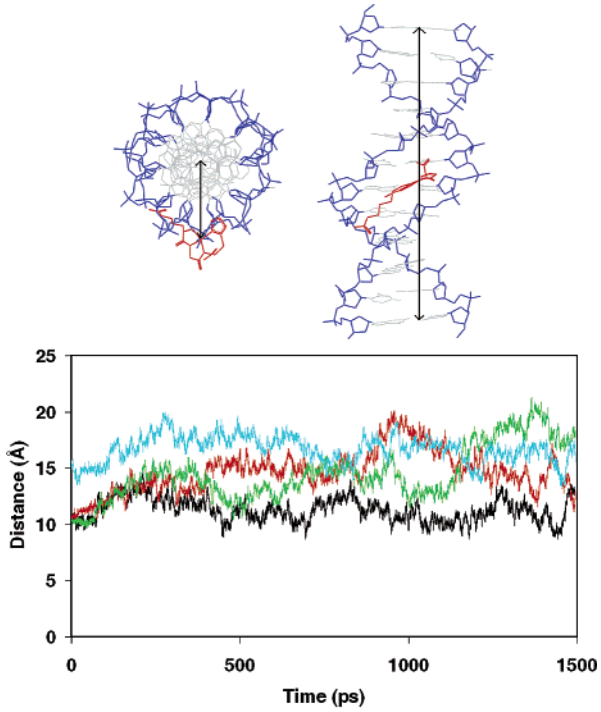

Figure 5. Definition of the distance between the Ni^{2+} of Ni(II)•L-Arg-Gly-His and the central axis of d(CGCGAATTCGCG)$_2$ (upper panel) and changes in the distance between Ni^{2+} and the central axis from the simulation of Ni(II)•L-Arg-Gly-His bound to d(CGCGAATTCGCG)$_2$ in four orientations (lower panel): **I**, black; **II**, red; **III**, green; and **IV**, blue.

the depths of metallopeptide-minor groove binding, the changes in the distance between the central Ni^{2+} atom of Ni(II)•L-Arg-Gly-His and the helix axis of DNA (as defined in Figure 5) were determined from each simulation. A plot of this distance versus time (Figure 5) shows that Ni(II)•L-Arg-Gly-His is inserted deepest into the minor groove via orientation **I** compared to all other orientations. In conjunction with this measurement, an analysis of the distances between the DNA A6 C2 proton and the His imidazole ring C4 proton, the NOE partners reported earlier,[13] indicates that only in orientation **I** is this distance (∼3−5 Å) compatible with the observed NOE; in orientations **II**, **III**, and **IV**, these distances are ∼8, 10, and 15 Å, respectively. Further, an examination of the distances between the Ni^{2+} center of the metallopeptide and proximal C4′−H protons, likely targeted during DNA cleavage, indicates, again, that in orientation **I** these distances are most compatible with observed C4′−H abstraction chemistry; the averaged distances measured for orientations **I**, **II**, **III**, and **IV** were 3.6, 4.2, 4.4, and 7.6 Å, respectively.

Taken together, these observations suggest that the favored binding orientation of DNA-Ni(II)•L-Arg-Gly-His, like Ni(II)•Gly-Gly-His, is **I**, an orientation in which the metallopeptide equatorial plane is associated with the minor groove via the amino-terminal N−H, the pyrrole N−H of the His imidazole, and the side chain of Arg. Oriented as such, and with an occasional third point of contact provided by the Arg side chain, the interaction between the metallopeptide and the DNA is stronger than with Ni(II)•Gly-Gly-His, and this orientation not only holds the metallopeptide deeply in the minor groove but also narrows the width of the DNA minor groove.

Table 3. Relative Binding Energies of DNA + Ni(II)•L-Arg-Gly-His[a]

orientation	$\Delta E_{complex}$[b]	ΔE_{DNA}[b]	ΔE_{ligand}[b]	$\Delta\Delta E$[c]
I	0	0	0	0
II	62.6	−11.7	20.5	53.8
III	133.4	−15.3	19.1	129.6
IV	53.2	−53.1	5.4	100.9

[a] Energies are reported in kilocalories per mole. [b] $\Delta E_{complex}$, ΔE_{DNA}, and ΔE_{ligand} denote the molecular mechanical (MM) energies for the complex, DNA, and ligand, respectively, relative to orientation **I**. [c] Relative binding energies, calculated by $\Delta\Delta E = \Delta E_{complex} - \Delta E_{DNA} - \Delta E_{ligand}$.

The outcome described above is consonant with the relative binding energies of Ni(II)•L-Arg-Gly-His shown in Table 3 where the simulation resulting from **I** is most stable. The binding energy of **III** is much higher than all others, indicating that the intermolecular interaction resulting from this initial orientation, in which H-bond *acceptors* are presented by the metallopeptide to the floor of the minor groove, a completely opposite scenario in comparison to **I**, is weaker. As shown in Table 3, the relative binding energies resulting from orientations **II** and **IV** show that they are significantly less stable than that obtained for **I**.

Further Analysis and Comparison of the Simulations of DNA + Ni(II)•Gly-Gly-His and DNA + Ni(II)•L-Arg-Gly-His Initiated from Orientation I. Further analyses of the simulations of DNA-Ni(II)•Gly-Gly-His and DNA-Ni(II)•L-Arg-Gly-His initiated from **I** were carried out in light of our initial findings. Illustrated in Figure 6 are the RMS deviations of the DNA-Ni(II)•Gly-Gly-His complex, the DNA alone, and the metallopeptide alone relative to the starting structure of Ni(II)•Gly-Gly-His bound to the DNA minor groove in orientation **I**. These results indicate that (1) the RMSDs of the DNA-Ni(II)•Gly-Gly-His complex and of the DNA alone have identical patterns of change, suggesting that Ni(II)•Gly-Gly-His did not move substantially along the minor groove and that the major structural changes attributable to the RMS deviations of the metallopeptide + DNA complex system derive from the flexibility of the DNA backbone and (2) the RMSDs of the DNA + metallopeptide

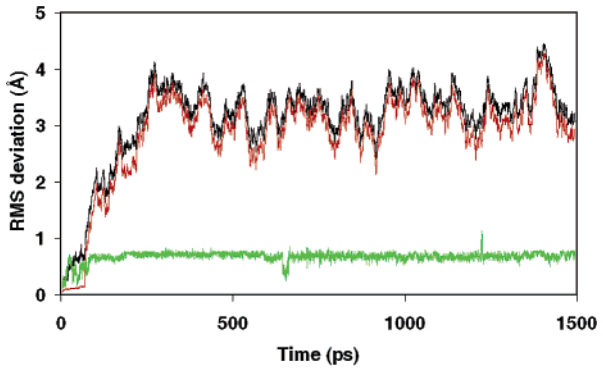

Figure 6. RMS deviations of DNA + Ni(II)•Gly-Gly-His (black), DNA alone (red), and metallopeptide alone (green) with respect to the starting structure in orientation **I** in the simulation of Ni(II)•Gly-Gly-His bound to d(CGCGAATTCGCG)$_2$.

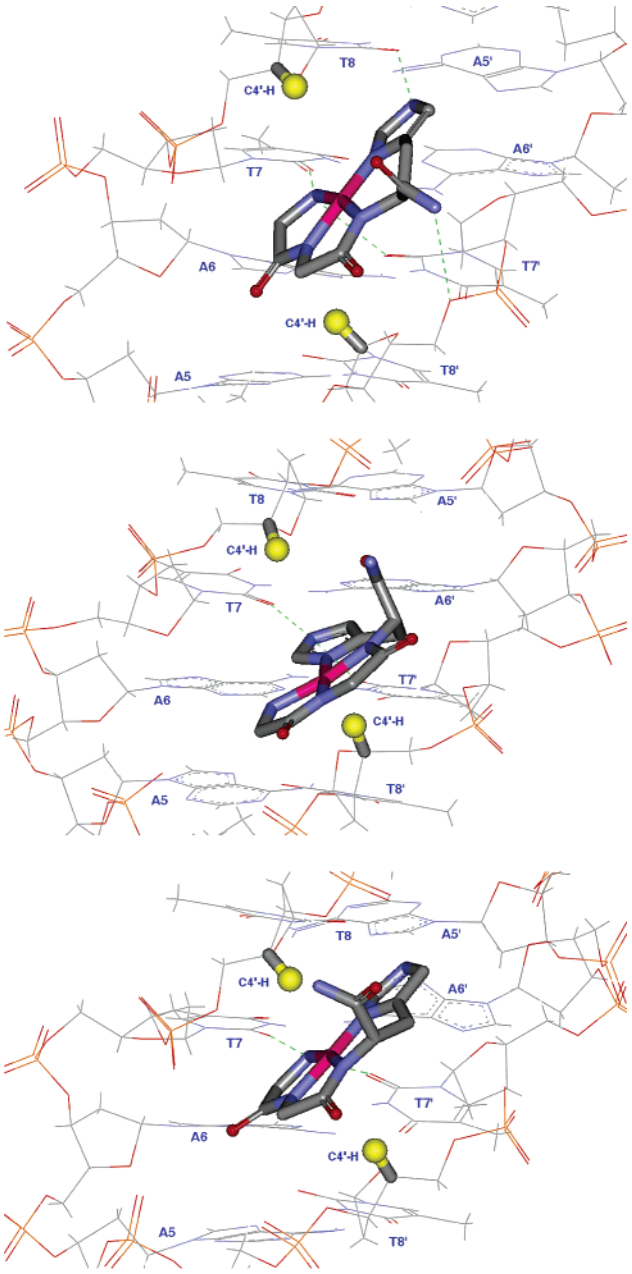

Figure 7. Snapshots of structures illustrating the H-bonds observed upon simulation of Ni(II)•Gly-Gly-His bound to d(CGCGAATTCGCG)$_2$ in orientation **I**. In these snapshots (1) the His imidazole and the amino-terminal amine are involved simultaneously in H-bonding to the O2 of T8 and O2 of T7 and T7′, respectively, while the carboxy-terminal amide N−H is occasionally associated with the O3′ of T7′ (upper panel); (2) the His imidazole pyrrole N−H interacts alone, as described above, with the floor of the minor groove (middle panel); and (3) the amino-terminal N−H interacts alone, as described above, with the floor of the minor groove (lower panel).

complex deviated consistently (∼0.2 Å) from that of DNA alone, while the average RMS value of Ni(II)•Gly-Gly-His is small (∼0.69 Å), indicating that the motion of the DNA-bound Ni(II)•Gly-Gly-His remained somewhat independent of the DNA groove, a result arising from a weakened intermolecular interaction. This observation is entirely

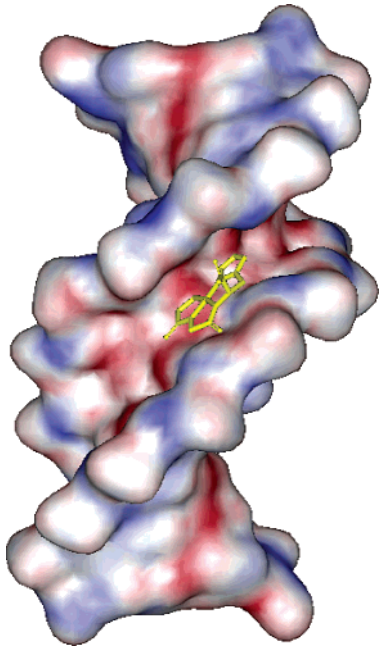

Figure 8. Space filling DNA model of the average structure of Ni(II)•Gly-Gly-His bound to d(CGCGAATTCGCG)$_2$ in orientation **I** emphasizing the binding orientation of the metallopeptide within the DNA minor groove and the resulting groove widths.

consistent with the random and inefficient DNA cleavage data found in previous experimental studies.[5]

In light of the dynamic motions described earlier, an analysis of the intermolecular contacts that form between the DNA and the metallopeptide in orientation **I** indicated that Ni(II)•Gly-Gly-His formed H-bonds to acceptors on the floor of the DNA minor groove via the amino-terminal N−H protons to O2 of T7, O2 of T7′ and O4′ and O5′ of T8 (32% of the simulation time), the N−H of the His imidazole pyrrole to O2 and O2P of T8 (7% of the simulation time), and the carboxyl-terminal amide protons to O2P, O5′ of T8′, and O3′ of T7 or the phosphate moiety of T7 and T8′ (17% of the simulation time). Figure 7 illustrates the above through snapshots of structures that occur in the simulation initiated from **I** showing the H-bonds formed between the DNA minor groove and Ni(II)•Gly-Gly-His. In addition, as shown in Figure 8, we note that the DNA backbone is relatively stable during the course of the simulation without visible bending, but, as a consequence of metallopeptide binding, the minor groove width slightly widens to 11.4 Å in comparison to the DNA alone (10.4 Å).[18]

For comparison to Ni(II)•Gly-Gly-His, we illustrate in Figure 9 the RMSDs of the DNA-Ni(II)•L-Arg-Gly-His complex, the DNA alone, and the metallopeptide alone relative to the starting structure of Ni(II)•L-Arg-Gly-His bound to the DNA minor groove in orientation **I**. The deviations found for this system differ from those of DNA + Ni(II)•Gly-Gly-His discussed earlier. The RMSDs of Ni(II)•L-Arg-Gly-His and the DNA alone coincided precisely during the simulation without the consistent deviation observed in the case of Ni(II)•Gly-Gly-His. This observation suggests that Ni(II)•L-Arg-Gly-His fits snugly into the minor groove with very little independent motion. The metallopep-

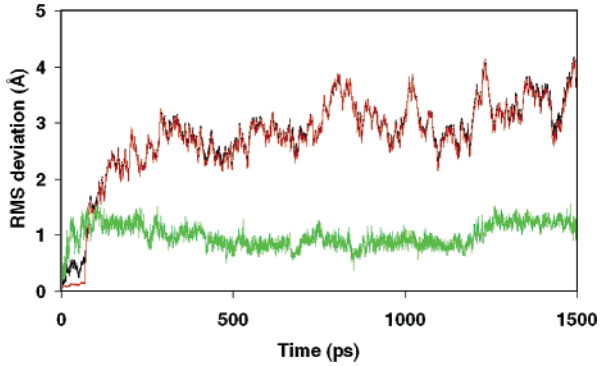

Figure 9. RMS deviations of Ni(II)•L-Arg-Gly-His + DNA (black), DNA alone (red), and Ni(II)•L-Arg-Gly-His alone (green) with respect to the starting structure in orientation **I** in the simulations of Ni(II)•L-Arg-Gly-His bound to d(CGCGAATTCGCG)$_2$.

tide moves and flexes with the motion of the DNA backbone during the course of the simulation and the structural changes of both the metallopeptide and the DNA backbone contributed to the RMS deviations of the whole complex. The DNA-Ni(II)•L-Arg-Gly-His complex has a lower averaged RMSD (∼3.11 Å), and Ni(II)•L-Arg-Gly-His alone has a higher RMSD (∼1.46 Å) compared to the corresponding values for Ni(II)•Gly-Gly-His (∼3.37 and 0.69 Å, respectively), indicating that the L-Arg isomer maintained a better overall complementary fit with the DNA during the course of the simulation, i.e., as the DNA flexed, the Ni(II)•L-Arg-Gly-His metallopeptide was capable of moving with it due to its stronger interactions with the minor groove.

Illustrating the above, Figure 10 shows a space filling DNA model of the average structure resulting from the simulation of Ni(II)•L-Arg-Gly-His bound initially to d(CGCGAATTCGCG)$_2$ in orientation **I**. As shown, Ni(II)•L-Arg-Gly-His fits in the minor groove at the dyad of the A/T-rich region with the equatorial plane of the metallopeptide residing parallel to the walls of the minor groove and with the central Ni^{2+} of the complex equidistant from two proximal cross-strand C4′−H protons, as noted earlier. While the equatorial plane of the complex is docked in the minor groove, the Arg side chain extends along the minor groove and interacts transiently with H-bond acceptors at the junction between the A/T-rich central core of the oligonucleotide and the flanking G/C-rich termini. As also noted earlier, the width of the minor groove at the center of the A/T-rich region is narrowed (from 10.4 to 9.7 Å)[18] upon interaction of the DNA and metallopeptide, while the width of the minor groove at the G/C−A/T junction was widened (from 10.4 to 16.8 Å) due to the transition of the phosphate diesters at that location (A_6 and G_{10}′) from B_{II} to B_I.[15,19]

Along with the gross structure changes, an analysis of the H-bonds that form between Ni(II)•L-Arg-Gly-His and the A/T region of the minor groove (Figure 10) revealed differences when compared to those observed for Ni(II)•Gly-Gly-His + DNA. The key difference is that the longest-lived H-bonds formed between the DNA and Ni(II)•L-Arg-Gly-His were due to the imidazole pyrrole N−H and the amino-terminal peptide N−H protons to H-bond acceptors on the floor of the minor groove, which include the N3 of adenine

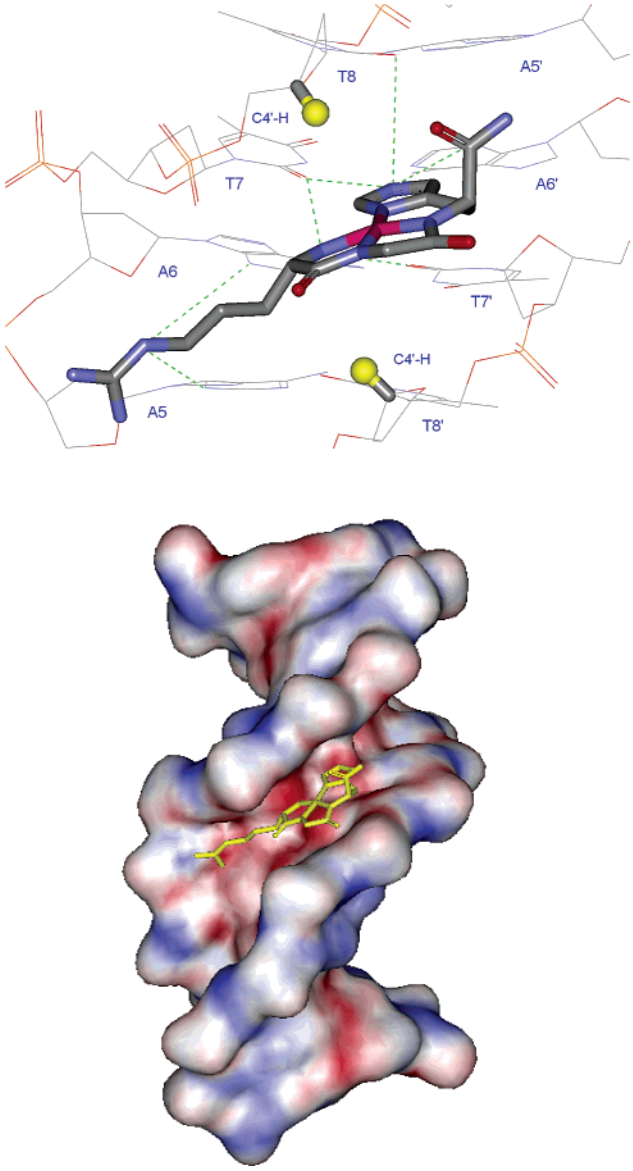

Figure 10. Average structures illustrating the H-bonds observed upon simulation of Ni(II)•L-Arg-Gly-His bound to d(CGCGAATTCGCG)$_2$ via orientation **I** (upper panel) and a space filling DNA model (lower panel) from the same simulation emphasizing the binding orientation of the metallopeptide within the DNA minor groove and the resulting groove width.

and O2 of thymine on both DNA strands (up to 80% of the simulation time). The stability of these interactions is greater than the same, albeit transient, interactions that occur between the minor groove and Ni(II)•Gly-Gly-His. Due to the L-stereochemistry of the Arg side chain, the overall curvature of Ni(II)•L-Arg-Gly-His complemented well the curvature of the minor groove and allowed the amino-terminal N−H protons to explore and form H-bonds to the O2 of two thymine residues in the center of the AATT sequence. Along with the imidazole N−H and amino-terminal N−H interactions, which locked Ni(II)•L-Arg-Gly-His deeply in the AATT core region, the positively charged side chain guanidinium group extended beyond the AATT core region and interacted with the DNA at the junction between the G4•C9′ and A5•T8′ base pairs (via the N3 and phosphate moiety O2P, O3′, and O5′ of A5 and A6). The Arg side chain also

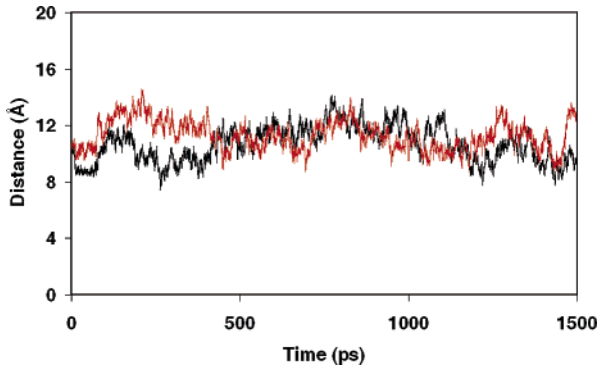

Figure 11. Changes in the distance between metallopeptide-bound Ni^{2+} and the central axis of DNA during the simulation of Ni(II)•Gly-Gly-His (black) and Ni(II)•L-Arg-Gly-His (red) bound to $d(CGCGAATTCGCG)_2$ in orientation **I**.

assisted in maintaining the core equatorial plane of the metallopeptide in orientation **I**. Indeed, the above two factors, stereochemistry and electrostatics, confer a distinct stabilizing advantage to the L-Arg-containing metallopeptide system in comparison to the Gly-only metallopeptide.

With the interactions described above, the distance (noted earlier) between the Ni(II)•L-Arg-Gly-His imidazole C4 proton and the minor groove A6-C2 proton ranges from 3 to 5 Å, consistent with the intermolecular NOE observed to occur between these two protons in the NMR study of DNA-Ni(II)•L-Arg-Gly-His.[13] In addition, the distances from the Ni(II) center to the T7 and T8 C5-methyl groups were 5.5 and 6.7 Å, respectively, again corresponding to the NMR data. Previous NMR studies also indicated a slight perturbation in the G•C base pairs flanking the AATT core of the oligonucleotide consistent with the point of Arg side chain contact observed in the present study.

Even though the binding of Ni(II)•Gly-Gly-His and Ni(II)•L-Arg-Gly-His in orientation **I** to the minor groove of DNA have apparent differences, they both insert into the minor groove to comparable depths (as shown in Figure 11). This insertion leads to a positioning of the central Ni^{2+} ion of each complex approximately equidistant between the T8 and T8′ C4′−H protons located on complementary DNA strands with the square-plane parallel to the walls of the minor groove. These observations account for the fact that despite the instability of the minor groove interaction displayed by Ni(II)•Gly-Gly-His vs Ni(II)•L-Arg-Gly-His, both metallopeptides share a common pathway leading to DNA cleavage via C4′−H abstraction; indeed, the C4′−H is prominently displayed in the minor groove[25] and readily accessible by either metallopeptide relative to other deoxyribose positions.

The above observations are consistent with, and assist in explaining, the ability of both Ni(II)•Gly-Gly-His and Ni(II)•L-Arg-Gly-His to interact with DNA, albeit with differing stabilities and cleavage efficiencies. These differences also rationalize the experimentally determined site-selectivites of these two distinct metallopeptides: Ni(II)•Gly-Gly-His results in relatively nonselective, inefficient DNA strand scission via C4′−H abstraction, while Ni(II)•L-Arg-Gly-His cleaves a subset of available nucleotides within a given A/T-rich site, indicating a more selective and stabilized association with the minor groove.[13]

Conclusions

Implications for Understanding DNA Recognition and Cleavage. Molecular dynamics simulations were carried out to examine all reasonably possible orientations of DNA minor groove binding by Ni(II)•Xaa-Gly-His metallopeptides. This investigation indicated that the most likely minor groove binding orientation for both metallopeptides is orientation **I**, through which both metallopeptides bind to the DNA minor groove deeper and with lower binding energies in comparison to other possibilities. Among the interactions found to occur between the minor groove of DNA and a metallopeptide, the N−H group of the His imidazole plays an important role by functioning as an H-bond donor to the N3 of adenine residues and the O2 of thymine residues located on the floor of the minor groove. The amino-terminal N−H also assists in metallopeptide-minor groove recognition and association in conjunction with the stereochemistry and chemical nature of the amino acid side chain substituted at this position.[14,15] In the presence of a positively charged L-Arg side chain, DNA recognition and affinity is enhanced through an increased electrostatic interaction, favorable stereochemical interactions, and the ability to mediate a third point of contact with the floor of the minor groove; this stabilizing factor is absent in Ni(II)•Gly-Gly-His.

As a consequence of binding orientation (**I**), our analyses indicate that the reactive metal center of each Ni(II)•Xaa-Gly-His metallopeptide is held in close proximity to known target C4′−H protons of the DNA. Abstraction of these protons via 1 or 2 e^- oxidation[8] leads either to a radical or cationic C4′ nucleotide lesion, respectively, and ultimately DNA strand scission. The observations made in the current investigation also correlate well to the efficiencies of DNA strand scission observed experimentally: Ni(II)•Arg-Gly-His is more efficient at C4′−H abstraction than Ni(II)•Gly-Gly-His. Noteworthy also is the fact that Ni(II)•Arg-Gly-His [or Ni(II)•Lys-Gly-His] generates fewer single electron abstraction products relative to Ni(II)•Gly-Gly-His;[8] single electron abstraction products require rapid recombination with O_2, which is likely blocked by the more stable DNA-Ni(II)•Arg-Gly-His interaction found in orientation **I**. Overall, these findings reinforce the importance of complementary H-bonding, multiple points of drug−DNA contact, and stable positioning of a catalytic center relative to a target atom in the design of reactive minor groove binding agents. Low molecular weight examples illustrating these factors are important toward the development of improved DNA targeted agents and our understanding of DNA recognition phenomena.

Acknowledgment. We thank the National Institutes of Health for financial support of this work (GM 62831 to E.C.L.). In addition, one of us (Y.-Y. F.) would like to acknowledge funding from the National Institutes of Health (G12 RR003048 from the RCMI program, Division of

Research Infrastructure, National Center for Research Resources to Howard University).

References

(1) Sigman, D. S.; Mazumder, A.; Perrin, D. M. Chemical nucleases. *Chem. Rev.* **1993**, *93*, 2295−2316.

(2) Pyle, A. M.; Barton, J. K. Probing nucleic acids with transition metal complexes. *Prog. Inorg. Chem*. **1990**, *38*, 413−475.

(3) Long, E. C. The DNA helical biopolymer: A template for the binding, assembly, and reactivity of metal ions and complexes. *J. Inorg. Organomet. Polym*. **1993**, *3*, 3−39.

(4) Neidle, S. DNA minor-groove recognition by small molecules. *Nat. Prod. Rep*. **2001**, *18*, 291−309.

(5) Long, E. C.; Claussen, C. A. DNA and RNA recognition and modification by Gly-Gly-His-derived metallopeptides. In *DNA and RNA Binders: From Small Molecules to Drugs*; Demeunynk, M., Bailly, C., Wilson, W. D., Eds.; Wiley-VCH: New York, 2003; pp 88−125.

(6) Long, E. C. Ni(II)•Xaa-Xaa-His metallopeptide DNA/RNA interactions. *Acc. Chem. Res*. **1999**, *99*, 827−836.

(7) Claussen, C. A.; Long, E. C. Nucleic acid recognition by metal complexes of bleomycin. *Chem. Rev*. **1999**, *99*, 2797−2816.

(8) Liang, Q.; Ananias, D. C.; Long, E. C. Ni(II)•Xaa-Xaa-His induced DNA cleavage: Deoxyribose modification by a common "activated" intermediate derived from $KHSO_5$, MMPP, or H_2O_2. *J. Am. Chem. Soc*. **1998**, *120*, 248−257.

(9) Jin, Y.; Cowan, J. A. DNA cleavage by copper-ATCUN complexes. Factors influencing cleavage mechanism and linearization of dsDNA. *J. Am. Chem. Soc*. **2005**, *127*, 8408−8415.

(10) Kimoto, E.; Tanaka, H.; Gyotoku, J.; Morishige, F.; Pauling, L. Enhancement of antitumor activity of ascorbate against Ehrlich ascites tumor cells by the copper:glycylglycylhistidine complex. *Cancer Res*. **1983**, *43*, 824−828.

(11) Licini, G.; Scrimin, P. Metal-ion binding peptides: From catalysis to protein tagging. *Angew. Chem., Int. Ed*. **2003**, *42*, 4572−4575.

(12) Nagane, R.; Koshigoe, T.; Chikira, M.; Long, E. C. The DNA-bound orientation of Cu(II)•Xaa-Gly-His metallopeptides. *J. Inorg. Biochem*. **2001**, *83*, 17−23.

(13) Fang, Y.-Y.; Ray, B. D.; Claussen, C. A.; Lipkowitz, K. B.; Long, E. C. Ni(II)•Arg-Gly-His-DNA interactions: Investigation into the basis for minor-groove binding and recognition. *J. Am. Chem. Soc*. **2004**, *126*, 5403−5412.

(14) Liang, Q.; Eason, P. D.; Long, E. C. Metallopeptide-DNA interactions: Site-selectivity based on amino acid composition and chirality. *J. Am. Chem. Soc*. **1995**, *117*, 9625−9631.

(15) Fang, Y.-Y.; Claussen, C. A.; Lipkowitz, K. B.; Long, E. C. Diastereoselective DNA cleavage recognition by Ni(II)•Gly-Gly-His derived metallopeptides. *J. Am. Chem. Soc*. **2006**, *128*, 3198−3207.

(16) Harford, K.; Sarkar, B. Amino terminal Cu(II)- and Ni(II)-binding (ATCUN) motif of proteins and peptides: Metal binding, DNA cleavage, and other properties. *Acc. Chem. Res*. **1997**, *30*, 123−130.

(17) Wellenzohn, B.; Winger, R. H.; Hallbrucker, A.; Mayer, E.; Liedl, K. R. Simulation of *Eco*RI dodecamer netropsin complex confirms class I complexation mode. *J. Am. Chem. Soc*. **2000**, *122*, 3927−3931.

(18) Wellenzohn, B.; Flader, W.; Winger, R. H.; Hallbrucker, A.; Mayer, E.; Liedl, K. R. Significance of ligand tails for interaction with the minor groove of B-DNA. *Biophys. J*. **2001**, *81*, 1588−1599.

(19) Flader, W.; Wellenzohn, B.; Winger, R. H.; Hallbrucker, A.; Mayer, E.; Liedl, K. R. $B_I - B_{II}$ substrate transitions induce changes in the hydration of B-DNA, potentially mediating signal transduction from the minor to major groove. *J. Phys. Chem. B* **2001**, *105*, 10379−10387.

(20) Mohamadi, F.; Richardson, N. G. J.; Guida, W. C.; Liskamp, R.; Lipton, M.; Caufield, C.; Chang, G.; Hendrickson, T.; Still, W. C. MacroModel − an integrated software system for modeling organic and bioorganic molecules using molecular mechanics. *J. Comput. Chem.* **1990**, *11*, 440−467.

(21) *Spartan02*; Wavefunction, Inc.: Irvine, CA, 2002.

(22) Case, D. A.; Pearlman, D. A.; Caldwell, J. W.; Cheatham, T. E., III.; Wang, J.; Ross, W. S.; Simmerling, C. L.; Darden, T. A.; Merz, K. M.; Stanton, R. V.; Cheng, A. L.; Vincent, J. J.; Crowley, M.; Tsui, V.; Gohlke, H.; Radmer, R. J.; Duan, Y.; Pitera, J.; Massova, I.; Seibel, G. L.; Singh, U. C.; Weiner, P. K. and Kollman, P. A. *AMBER 7*; University of California: San Francisco, CA, 2002.

(23) Sriram, M.; van der Marel, G. A.; Roelen, H. L.; van Boom, J. H.; Wang, A. H. J. Structural consequences of a carcinogenic alkylation lesion on DNA: Effect of O6-ethylguanine [e6G] on the molecular structure of d(CGC[e6G]AATTCGCG)-netropsin complex. *Biochemistry* **1992**, *31*, 11823−11834.

(24) Bal, W.; Djuran, M. I.; Margerum, D. W.; Gray, E. T.; Mazid, M. A.; Tom, R. T.; Nieboer, E.; Sadler, P. J. Dioxygen-induced decarboxylation and hydroxylation of [Ni^{II}(glycyl-glycyl-L-histidine)] occurs via Ni^{III}: X-ray crystal structure of [Ni^{II}(glycyl-glycyl-hydroxy-D,L-histamine)]•$3H_2O$. *J. Chem. Soc., Chem. Commun*. **1994**, 1889−1890.

(25) Knapp, W.; Tullius, T. D. Oxidative strand scission of nucleic acids: Routes initiated by hydrogen abstraction from the sugar moiety. *Chem. Rev*. **1998**, *98*, 1089−1107.

CT600074R